

# Quantum theory of polariton weak lasing and polarization bifurcations

Huawen Xu\* and Timothy C. H. Liew†

Division of Physics and Applied Physics, School of Physical and Mathematical Sciences,  
Nanyang Technological University, 21 Nanyang Link, Singapore 637371, Singapore

Yuri G. Rubo‡

Instituto de Energías Renovables, Universidad Nacional Autónoma de México, Temixco, Morelos, 62580, Mexico

(Dated: October 26, 2023)

The quantum theory of polariton condensation in a trapped state reveals a second-order phase transition evidenced by spontaneous polarization parity breaking in sub-spaces of fixed polariton occupation numbers. The emission spectra of polariton condensate demonstrate the coexistence of the symmetry-conserving condensate state with the linear X polarization and the symmetry-broken, elliptically polarized states in the vicinity of the threshold. As a result, the oscillating linear second-order coherence  $g_{xx}^{(2)}(t)$ , with  $g_{xx}^{(2)}(t) < 1$  over some time intervals, is obtained. The spontaneous symmetry breaking is reflected in the second-order cross correlator of circular polarizations. The related build-up of elliptically-polarized weak lasing results also in non-monotonous dependence of the circular second-order coherence on the excitation power and the interaction strength.

*Introduction.*—The experimental realization of optically trapped polariton condensates [1, 2] marked an important technological advance by allowing better control of condensate arrangement, polarization, and their mutual coupling. Positioning polariton condensates away from the excitation spots in the microcavity plane reduces substantially the thermal noise and the condensate decoherence, thus narrowing the polariton lasing lines. Combined with the recent progress in increasing the polariton lifetimes [3, 4] this makes networks of trapped condensates a promising platform for all-optical devices [5, 6] and neuromorphic computing [7–11].

Polariton condensates can encode information through their polarization (spin) state, which exhibits a great amount of interesting properties [12–15]. While at high excitation level the linearly polarized condensates are formed, the polarization state near the condensation threshold is more complex. It was discovered [16, 17] that a single trapped polariton condensate undergoes parity breaking bifurcation leading to random formation of two possible states of elliptically polarized condensates with opposite handedness. The polarization bifurcation near the threshold can be understood as the weak lasing effect: formation of specific many-body polariton states due to the combined effect of weak polariton-polariton repulsion and a small difference in the lifetimes of single-polariton states [18]. The mean-field theory used so far to describe this phenomenon studies the polariton condensation in terms of nonlinear driven-dissipative equations, where different condensate states correspond to fixed points or limit cycles [19, 20] (sometimes referred to as time crystals [21]). This theory lacks the ability to properly address the possible coexistence of condensates near the threshold and their quantum properties, which

are speculated to allow a quantum speed-up of polariton simulators [22]. Moreover, the validity of the mean-field description of weak lasing is limited by the assumption of weak polariton-polariton interaction. An essential property of weak lasing is that the formation of a condensate is stabilized by the interaction, not by the depletion of an incoherent feeding reservoir. As a result, the condensate occupation numbers are inversely proportional to the interaction constant. The latter is controlled by the condensate confinement, so that the requirement of weak interaction is a severe limitation.

In this Letter we discuss the properties of the trapped polariton condensate density matrix in the presence of the weak lasing effect. The system in this case obeys open-dissipative quantum dynamics described by the Lindblad master equation for the density matrix. We analyze properties of both the steady state solution and the different two-time correlators, as well as the emission spectrum from the condensate, and show how they indicate the symmetry breaking transition in the system and coexistence of condensates with different symmetries.

*Formalism.*—For a trapped condensate, we denote by  $\hat{a}$  and  $\hat{b}$  the annihilation operators for X and Y linearly polarized states, respectively, and assume different dissipation rates,  $\Gamma + \gamma$  and  $\Gamma - \gamma$ , from these states. If the polariton harvest rate  $W$  is polarization independent, the condensate density matrix  $\rho$  evolves according to the equation ( $\hbar = 1$ )

$$\begin{aligned} \frac{d\hat{\rho}}{dt} \equiv \mathcal{L}\hat{\rho} = & -i[\hat{H}, \hat{\rho}] - \frac{W}{2}([\hat{a}, \hat{a}^\dagger \rho] + [\hat{b}, \hat{b}^\dagger \rho] + \text{h.c.}) \\ & - \frac{(\Gamma + \gamma)}{2}([\hat{a}^\dagger, \hat{a} \rho] + \text{h.c.}) - \frac{(\Gamma - \gamma)}{2}([\hat{b}^\dagger, \hat{b} \rho] + \text{h.c.}). \end{aligned} \quad (1)$$

Here the coherent evolution of polariton condensate is

\* huawen.xu@ntu.edu.sg

† timothyliew@ntu.edu.sg

‡ ygr@ier.unam.mx

given by the Hamiltonian of the Bose-Hubbard dimer [23]

$$\hat{H} = -\frac{\varepsilon}{2}(\hat{\psi}_{+1}^\dagger \hat{\psi}_{-1} + \hat{\psi}_{-1}^\dagger \hat{\psi}_{+1}) + \frac{\alpha_1}{4}(\hat{\psi}_{+1}^{\dagger 2} \hat{\psi}_{+1}^2 + \hat{\psi}_{-1}^{\dagger 2} \hat{\psi}_{-1}^2) + \frac{\alpha_2}{2}\hat{\psi}_{+1}^\dagger \hat{\psi}_{-1}^\dagger \hat{\psi}_{+1} \hat{\psi}_{-1}, \quad (2)$$

where we use the operators  $\hat{\psi}_{\pm 1} = (\hat{a} \pm \hat{b})/\sqrt{2}$  for the circular polarization components, and  $\alpha_1$  and  $\alpha_2$  are the interaction constants for polaritons with the same and the opposite circular polarizations.

In what follows, it is convenient to introduce also the spin of the condensate, which is defined by the operators

$$\hat{s}_1 = \frac{1}{2}(\hat{a}^\dagger \hat{a} - \hat{b}^\dagger \hat{b}), \quad \hat{s}_2 = \frac{i}{2}(\hat{a}^\dagger \hat{b} - \hat{b}^\dagger \hat{a}), \quad (3a)$$

$$\hat{s}_3 = \frac{1}{2}(\hat{a}^\dagger \hat{b} + \hat{b}^\dagger \hat{a}), \quad \hat{s}_0 = \frac{1}{2}(\hat{a}^\dagger \hat{a} + \hat{b}^\dagger \hat{b}). \quad (3b)$$

With the aid of spin components, the Hamiltonian (2) can be written as

$$\hat{H} = \hat{H}_0 + \hat{H}_s, \quad \hat{H}_s = -\varepsilon \hat{s}_1 + \frac{\alpha}{2} \hat{s}_3^2, \quad (4)$$

where  $\alpha = \alpha_1 - \alpha_2$ . The Hamiltonian  $\hat{H}_s$  is recognized as the Lipkin-Meshkov-Glick model [24], while  $\hat{H}_0 = [\alpha_1 \hat{s}_0(\hat{s}_0 - 1) + \alpha_2 \hat{s}_0^2]/2$  depends only on the total spin operator  $\hat{s}_0$ , which defines the total number of polaritons in the condensate. The dynamical properties of the Hamiltonians  $\hat{H}$  and  $\hat{H}_s$  are the same. It is seen from the equation (1) that the density matrix possesses the block-diagonal structure: the  $1 \times 1$  block for the empty condensate, the  $2 \times 2$  block for one polaritons (spin  $1/2$ ), the  $3 \times 3$  block for two polaritons (spin 1), etc. Each block evolves independently of the others under the Hamiltonian term in (1), but the neighboring blocks are coupled by the drive-dissipation Lindblad terms in (1).

*Equilibrium condensate properties.*—From Eq. 1, one can note that in this system, instead of having a specific condensation threshold, we have a threshold region from  $W = \Gamma - \gamma$  to  $W = \Gamma + \gamma$ . Moreover, due to quantum fluctuations the condensate is already formed for  $W < \Gamma - \gamma$ . The semiclassical dynamics of the average spin components  $S_\mu = \langle \hat{s}_\mu \rangle$  (see the Supplemental Material [25] for the details) reveals the presence of the second order phase transition. For small pumping  $W$ , the condensate is formed with the Y polarization, but for  $W > W_c$  this state becomes unstable and two elliptically polarized condensates can appear with equal probability. This symmetry breaking manifests the weak lasing regime. The critical value  $W_c$  is close to  $\Gamma - \gamma$  for  $\alpha \ll 1$ , and it shifts to smaller values with increasing interaction constant.

Clearly, a sharp phase transition only takes place in the limit of large condensate occupations, where the mean field approximation is valid. To investigate the polarization parity breaking phenomenon at strong interaction and low occupation numbers, we evolve the master

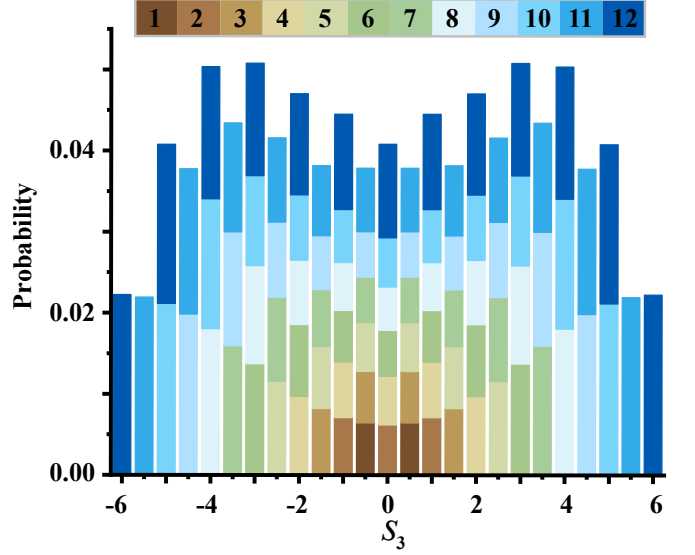


FIG. 1. Probability distribution of  $s_3$  with different contribution from states with different number of particles, where the numbers  $1, 2, \dots, 12$  (encoded by different colors) indicate the number of particles in a certain subspace of the system. The contribution from the vacuum state  $|0, 0\rangle$  is excluded. We have considered 12 maximum particles on each site,  $\Gamma = 1$ ,  $\gamma = 0.5$ ,  $W = 0.95$ ,  $\alpha = 1$ , and  $\varepsilon = 1$ .

equation (1) until reaching the steady state  $\hat{\rho}_0$ . Then we check the probability distribution of the spin operator  $\hat{s}_3$ . In the circular  $\hat{\psi}_{\pm 1}$  basis, it can be written as  $\hat{s}_3 = (\hat{\psi}_{+1}^\dagger \hat{\psi}_{+1} - \hat{\psi}_{-1}^\dagger \hat{\psi}_{-1})/2$  and it determines the polariton occupation number difference between the right and the left circularly polarized polariton modes. Possible eigenvalues of  $\hat{s}_3$  are  $s_3 = 0, \pm 1/2, \pm 1, \pm 3/2, \dots$ , and without parity breaking the 0 eigenvalue has the highest probability (the polariton condensate is linearly polarized).

The probability distribution  $P(s_3)$  is given by

$$\begin{aligned} P(s_3) &= \sum_{n,m} \langle n, m | \rho_0 | n, m \rangle \delta_{n,m+2s_3} \\ &= \sum_n \langle n, n - 2s_3 | \rho_0 | n, n - 2s_3 \rangle, \end{aligned} \quad (5)$$

where  $n$  and  $m$  are the numbers of polaritons in the  $+1$  and  $-1$  states, respectively. We see from Fig. 1 that instead of centering at 0, the probability distribution shows a double-peak structure, indicating that the polaritons have higher chance to condense at either the right circularly polarized ( $s_3 > 0$ ) or the left circularly polarized ( $s_3 < 0$ ) states. This is the fingerprint of the polariton condensate undergoing a circular polarization parity symmetry breaking.

In Fig. 1, different colors in the stacked bar chart represent different contributions from states with different numbers of polaritons. For example, 1 represents the contribution from states with only one polariton ( $|0, 1\rangle$  and  $|1, 0\rangle$ ). Also, one can note that states with more po-

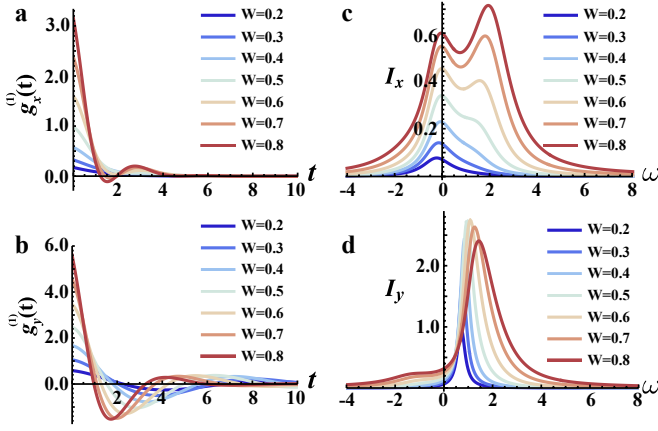


FIG. 2. Showing the first order correlation functions for the X polarization (a) and the Y polarization (b), under different pumping strength  $W$ . The corresponding emission spectra  $I_{x,y}(\omega)$  are shown in panels (c) and (d). We have considered 12 maximum polaritons on each site,  $\Gamma = 1$ ,  $\gamma = 0.5$ ,  $\alpha = 1$ ,  $\varepsilon = 1$ .

laritons have a more pronounced symmetry breaking, as the interactions between the polaritons are more significant.

*Emission spectra.*—Here we analyze how the polarization symmetry-breaking transition is reflected in the light emission spectra, that are directly related to experimental observations. To this aim, we consider the time-delayed first-order correlation functions for X and Y polarized polariton modes,

$$g_x^{(1)}(t) = \langle \hat{a}^\dagger(t) \hat{a}(0) \rangle, \quad g_y^{(1)}(t) = \langle \hat{b}^\dagger(t) \hat{b}(0) \rangle. \quad (6)$$

The time dependent correlators can be calculated in the framework of the quantum regression method [26]. Namely, to evaluate  $\langle \hat{A}(t) \hat{B}(0) \rangle$  we evolve the modified operator  $\hat{\rho}_B(0) = \hat{B}(0) \hat{\rho}_0$  to find  $\hat{\rho}_B(t) = e^{\mathcal{L}t} \hat{\rho}_B(0)$  using the Lindbladian superoperator  $\mathcal{L}$  from Eq. (1). Then,  $\langle \hat{A}(t) \hat{B}(0) \rangle = \text{Tr}\{\hat{A}(0) \hat{\rho}_B(t)\}$ .

The first-order coherence functions (6), shown in Fig. 2(a,b), decrease with the time delay corresponding to a finite coherence time in the system. It is natural that they also oscillate in time given the energy difference of the X and Y modes, that is also renormalized by different blue-shifts of these modes with increasing pumping. It can also be noted that the first order coherence time decreases slightly with stronger pumping strength  $W$ . This is expected given that under higher pumping strength the interaction between the polaritons becomes more important and it leads to additional dephasing [27].

The emission spectra for X and Y polarizations can be found as

$$I_{x,y}(\omega) = \frac{1}{\pi} \text{Re} \int_0^\infty g_{x,y}^{(1)}(t) e^{-i\omega t} dt, \quad (7)$$

and they are shown in Fig. 2(c,d). These spectra demonstrate features that are not expected from mean-field the-

ory [25]. The latter predicts only one emission peak, originating either for the symmetry conserving Y-polarized state, or from two symmetry breaking elliptically polarized states, that possess opposite handedness but the same emission frequency. The X-polarization spectra, however, clearly demonstrate coexistence of two different condensate states and corresponding two-peak structure. At low pumping, there is only emission line originating from the X-polarized condensate, that appears initially at  $\omega = -\varepsilon/2$  and is gradually blue-shifted with increasing pumping  $W$ . At moderate and strong pumping the second line becomes more and more important and it indicates the formation of weak lasing condensates. The blue-shift of different condensate states are different, with the blue-shift of weak lasing state been stronger, since it is more occupied. Consequently, at  $W = 0.8$  we see the superposition of two peaks, separated by some distance bigger than the Josephson splitting  $\varepsilon$ . Similarly, in the spectrum of Y polarized polaritons (Fig. 2(d)), we can see also a weak second peak appearing at the low-frequency wing of the much stronger weak lasing peak. It is not quite resolved since the emission from Y polarized polaritons is stronger, as they have smaller decay rate.

*The second-order correlators.*—Another experimentally important quantity is the second-order coherence. Here we calculate the time-dependent second-order correlation functions

$$g_{uv}^{(2)}(t) = \frac{\langle \hat{u}^\dagger(0) \hat{v}^\dagger(t) \hat{v}(t) \hat{u}(0) \rangle}{\langle \hat{u}^\dagger(0) \hat{u}(0) \rangle \langle \hat{v}^\dagger(t) \hat{v}(t) \rangle}. \quad (8)$$

where  $\hat{u}$  and  $\hat{v}$  could be  $\hat{a}$ ,  $\hat{b}$ , or the circular polarization operators  $\hat{\psi}_{\pm 1}$ .

The results for  $g_{yy}^{(2)}(t)$  and  $g_{xx}^{(2)}(t)$  are shown in Fig. 3. It can be seen that the second order coherence at zero time delay decreases from roughly 2 (corresponding to a thermal state) toward 1 (a coherent state) upon increasing the pumping strength. This is a generally expected of

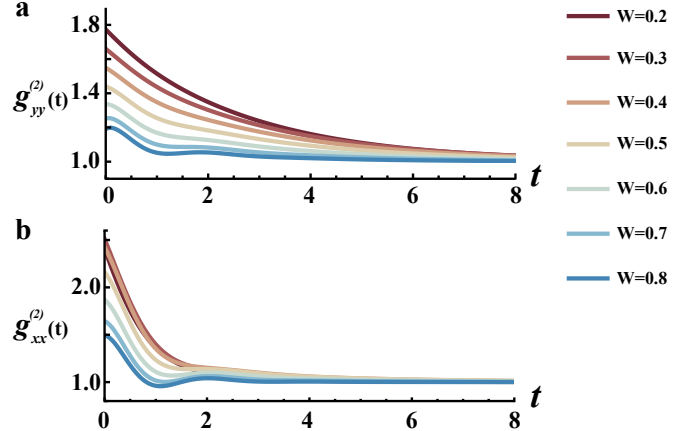


FIG. 3. The second order correlation function  $g_{yy}^{(2)}(t)$  [Y polarization, panel (a)] and  $g_{xx}^{(2)}(t)$  [X polarization, panel (b)] for different pumping strengths  $W$ . We have considered 12 maximum particles on each site,  $\Gamma = 1$ ,  $\gamma = 0.5$ ,  $\alpha = 1$ ,  $\varepsilon = 1$ .

polariton condensates, although we don't reach a perfect coherence due to the small numbers of particles involved. It can also be noted that the second order coherence of the Y polarization (the  $\hat{b}$  mode) exceeds that of the X polarization (the  $\hat{a}$  mode), and that there is an oscillation in the second order coherence taking place at higher pumping powers. Such oscillations are expected in coupled mode systems (e.g., in unconventional blockade systems [28]). Given that the mechanism in our present case of coupling  $\hat{a}$  and  $\hat{b}$  modes is via the nonlinear interaction term ( $\alpha$ ), it is reasonable that these oscillations only become significant at higher pumping powers. Let us further recall that the  $\hat{b}$  mode corresponds to the lower loss state and hence the state with higher number of particles. The  $\hat{b}$  mode acts then as a source of particles for the  $\hat{a}$  mode (even though the  $\hat{a}$  mode also receives particles directly from the pumping). We note that this source corresponds to terms of the form  $\hat{a}^\dagger \hat{a}^\dagger \hat{b} \hat{b}$ , which appear from the  $\hat{s}_3^2$  term. As the scattering rate of such a source term depends on the number of particles already in the  $\hat{a}$  state this term can be considered as a stimulated scattering term, which consequently imparts coherence to the mode being developed. This explains why the  $\hat{a}$  modes tend to have a smaller second order correlation function. Further, we note that it was previously shown in systems of bosonic cascades [29] that when a mode acquires coherence from another, the original source mode, which in our case is  $\hat{b}$ , should show more bunching. That is,  $\hat{b}$  can develop a higher second order correlation function as a result of the nonlinear coupling. Another interesting feature seen in Fig. 3(b) is the presence of time-intervals with of  $g_{xx}^{(2)}(t) < 1$ . This effect becomes more pronounced with increasing interaction, but it is still not sufficient to obtain the sub-Poissonian polariton statistics.

The polarization parity symmetry breaking can also be told from the second order cross correlator  $g_{cc}^{(2)}(t)$  of left and right circular polarized polaritons, which can be defined by setting  $\hat{u} = \hat{\psi}_{+1}$  and  $\hat{v} = \hat{\psi}_{-1}$  in Eq. (8). Such a coefficient provides information about the temporal correlations between the left ( $\hat{\psi}_{-1}$ ) and right ( $\hat{\psi}_{+1}$ ) circularly polarized modes, and it is shown in Fig. 4(a). The value  $g_{cc}^{(2)}(t) < 1$  tells us that if a particle is observed in one circular polarization, then it is less likely to detect another particle in the opposite circular polarization. For long time delay, this anti-correlation is washed out, as the right and the left circular polarization have equal realization probabilities.

In Fig. 4(b) we also show the zero-delay second-order coherence for the same circular polarization  $g_{cc}^{(2)}(0)$ , obtained with  $\hat{u} = \hat{v} = \hat{\psi}_{+1}$  in Eq. (8) (and, of course, the same  $g_{cc}^{(2)}(0)$  is obtained for  $\hat{u} = \hat{v} = \hat{\psi}_{-1}$ ). For small pumping, the second order coherence initially increases above 2 for weak interaction strength  $\alpha$ , but it becomes

substantially smaller than 2 for strongly interacting polaritons. In this case, the dependence on the pumping  $W$  is non-monotonous, with  $g_{cc}^{(2)}(0)$  approaching unity for large pumping, which manifests the polariton lasing.

*Conclusions.*—The theory of polariton condensation and spontaneous polarization formation is typically treated within the mean-field approximation, which explicitly assumes large occupation numbers of the condensate. In applications of polariton condensates it is often speculated that quantum fluctuations play a key role and can lead to quantum speedup of polaritonic devices [22]. Consequently, it is essential to generalize the fundamental theory of polariton condensation into the quantum realm accounting for such fluctuations. By performing exact quantum calculations of the condensate density matrix, the first and the second order coherence, as well as the emission spectra, we demonstrate that the condensate formation near the threshold is indeed more complex. In particular, it involves possible coexistence of the states with broken and unbroken parity symmetry. The weak lasing in quantum case is manifested by spontaneous polarization parity breaking across the different particle number subspaces, and it can be experimentally detected by measuring the second-order cross correlations of circular polarization components.

*Acknowledgements.*—H.X. and T.C.H.L. were supported by the Ministry of Education (Singapore) Tier 2 grant MOE-T2EP50121-0020. This work was also supported in part by PAPIIT-UNAM Grant No. IN108524.

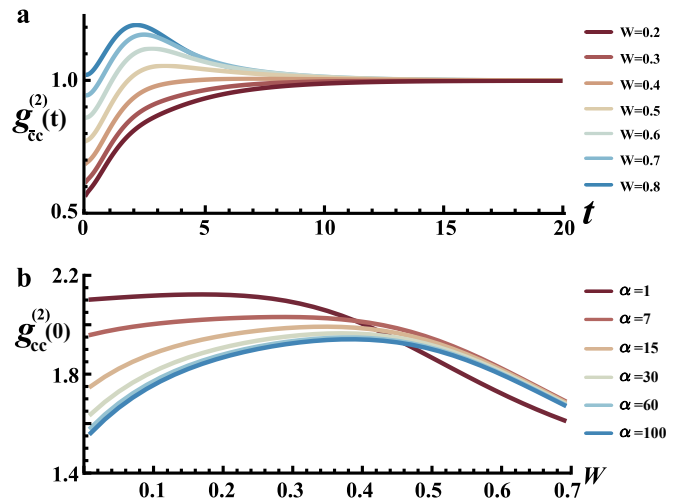


FIG. 4. (a) The time dependence of the second-order cross correlator  $g_{cc}^{(2)}(t)$  for different pumping strength  $W$ . (b) The second-order coherence  $g_{cc}^{(2)}(0)$  for the same circular polarization. We have considered 12 maximum particles on each site,  $\Gamma = 1$ ,  $\gamma = 0.5$ ,  $\varepsilon = 1$  for both panels, and  $\alpha = 1$  for panel (b).

---

[1] P. Cristofolini, A. Dreismann, G. Christmann, G. Franchetti, N. G. Berloff, P. Tsotsis, Z. Hatzopoulos, P. G. Savvidis, and J. J. Baumberg, Optical superfluid phase transitions and trapping of polariton condensates, *Phys. Rev. Lett.* **110**, 186403 (2013).

[2] A. Askitopoulos, H. Ohadi, A. V. Kavokin, Z. Hatzopoulos, P. G. Savvidis, and P. G. Lagoudakis, Polariton condensation in an optically induced two-dimensional potential, *Phys. Rev. B* **88**, 041308 (2013).

[3] S. Mukherjee, V. K. Kozin, A. V. Nalitov, I. A. Shelykh, Z. Sun, D. M. Myers, B. Ozden, J. Beaumariage, M. Steger, L. N. Pfeiffer, K. West, and D. W. Snoke, Dynamics of spin polarization in tilted polariton rings, *Phys. Rev. B* **103**, 165306 (2021).

[4] E. Estrecho, M. Pieczarka, M. Wurdack, M. Steger, K. West, L. N. Pfeiffer, D. W. Snoke, A. G. Truscott, and E. A. Ostrovskaya, Low-energy collective oscillations and Bogoliubov sound in an exciton-polariton condensate, *Phys. Rev. Lett.* **126**, 075301 (2021).

[5] D. Ballarini, M. De Giorgi, E. Cancellieri, R. Houdré, E. Giacobino, R. Cingolani, A. Bramati, G. Gigli, and D. Sanvitto, All-optical polariton transistor, *Nature Communications* **4**, 1778 (2013).

[6] D. Sanvitto and S. Kéna-Cohen, The road towards polaritonic devices, *Nature Materials* **15**, 1061 (2016).

[7] N. G. Berloff, M. Silva, K. Kalinin, A. Askitopoulos, J. D. Töpfer, P. Cilibrizzi, W. Langbein, and P. G. Lagoudakis, Realizing the classical XY Hamiltonian in polariton simulators, *Nature Materials* **16**, 1120 (2017).

[8] H. Ohadi, A. J. Ramsay, H. Sigurdsson, Y. del Valle-Inclan Redondo, S. I. Tsintzos, Z. Hatzopoulos, T. C. H. Liew, I. A. Shelykh, Y. G. Rubo, P. G. Savvidis, and J. J. Baumberg, Spin order and phase transitions in chains of polariton condensates, *Phys. Rev. Lett.* **119**, 067401 (2017).

[9] D. Ballarini, A. Gianfrate, R. Panico, A. Opala, S. Ghosh, L. Dominici, V. Ardizzone, M. De Giorgi, G. Lerario, G. Gigli, T. C. H. Liew, M. Matuszewski, and D. Sanvitto, Polaritonic neuromorphic computing outperforms linear classifiers, *Nano Letters* **20**, 3506 (2020).

[10] A. Opala and M. Matuszewski, Harnessing exciton-polaritons for digital computing, neuromorphic computing, and optimization [Invited], *Opt. Mater. Express* **13**, 2674 (2023).

[11] A. Kavokin, T. C. H. Liew, C. Schneider, P. G. Lagoudakis, S. Klembt, and S. Höefling, Polariton condensates for classical and quantum computing, *Nature Reviews Physics* **4**, 435 (2022).

[12] M. D. Martín, L. Viña, J. K. Son, and E. E. Mendez, Spin dynamics of cavity polaritons, *Solid State Communications* **117**, 267 (2001).

[13] P. G. Lagoudakis, P. G. Savvidis, J. J. Baumberg, D. M. Whittaker, P. R. Eastham, M. S. Skolnick, and J. S. Roberts, Stimulated spin dynamics of polaritons in semiconductor microcavities, *Phys. Rev. B* **65**, 161310 (2002).

[14] J. J. Baumberg, A. V. Kavokin, S. Christopoulos, A. J. D. Grundy, R. Butté, G. Christmann, D. D. Solnyshkov, G. Malpuech, G. Baldassarri Höger von Högersthal, E. Feltin, J.-F. Carlin, and N. Grandjean, Spontaneous polarization buildup in a room-temperature polariton laser, *Phys. Rev. Lett.* **101**, 136409 (2008).

[15] J. Levrat, R. Butté, T. Christian, M. Gläuser, E. Feltin, J.-F. Carlin, N. Grandjean, D. Read, A. V. Kavokin, and Y. G. Rubo, Pinning and depinning of the polarization of exciton-polariton condensates at room temperature, *Phys. Rev. Lett.* **104**, 166402 (2010).

[16] H. Ohadi, A. Dreismann, Y. G. Rubo, F. Pinsker, Y. del Valle-Inclan Redondo, S. I. Tsintzos, Z. Hatzopoulos, P. G. Savvidis, and J. J. Baumberg, Spontaneous spin bifurcations and ferromagnetic phase transitions in a spinor exciton-polariton condensate, *Phys. Rev. X* **5**, 031002 (2015).

[17] A. Dreismann, H. Ohadi, Y. del Valle-Inclan Redondo, R. Balili, Y. G. Rubo, S. I. Tsintzos, G. Deligeorgis, Z. Hatzopoulos, P. G. Savvidis, and J. J. Baumberg, A sub-femtojoule electrical spin-switch based on optically trapped polariton condensates, *Nature Materials* **15**, 1074 (2016).

[18] I. L. Aleiner, B. L. Altshuler, and Y. G. Rubo, Radiative coupling and weak lasing of exciton-polariton condensates, *Phys. Rev. B* **85**, 121301 (2012).

[19] S. Kim, Y. G. Rubo, T. C. H. Liew, S. Brodbeck, C. Schneider, S. Höfling, and H. Deng, Emergence of microfrequency comb via limit cycles in dissipatively coupled condensates, *Phys. Rev. B* **101**, 085302 (2020).

[20] R. Ruiz-Sánchez, R. Rechtman, and Y. G. Rubo, Autonomous chaos of exciton-polariton condensates, *Phys. Rev. B* **101**, 155305 (2020).

[21] A. V. Nalitov, H. Sigurdsson, S. Morina, Y. S. Krivosenko, I. V. Iorsh, Y. G. Rubo, A. V. Kavokin, and I. A. Shelykh, Optically trapped polariton condensates as semiclassical time crystals, *Phys. Rev. A* **99**, 033830 (2019).

[22] P. G. Lagoudakis and N. G. Berloff, A polariton graph simulator, *New Journal of Physics* **19**, 125008 (2017).

[23] F. P. Laussy, I. A. Shelykh, G. Malpuech, and A. Kavokin, Effects of bose-einstein condensation of exciton polaritons in microcavities on the polarization of emitted light, *Phys. Rev. B* **73**, 035315 (2006).

[24] H. J. Lipkin, N. Meshkov, and A. J. Glick, Validity of many-body approximation methods for a solvable model: (I). Exact solutions and perturbation theory, *Nuclear Physics* **62**, 188 (1965).

[25] See Supplemental Material for the semiclassical analysis.

[26] M. Lax, Formal theory of quantum fluctuations from a driven state, *Phys. Rev.* **129**, 2342 (1963).

[27] D. Porras and C. Tejedor, Linewidth of a polariton laser: Theoretical analysis of self-interaction effects, *Phys. Rev. B* **67**, 161310 (2003).

[28] T. C. H. Liew and V. Savona, Single photons from coupled quantum modes, *Phys. Rev. Lett.* **104**, 183601 (2010).

[29] T. C. H. Liew, Y. G. Rubo, A. S. Sheremet, S. D. Liberato, I. A. Shelykh, F. P. Laussy, and A. V. Kavokin, Quantum statistics of bosonic cascades, *New Journal of Physics* **18**, 023041 (2016).

**Supplemental Material**  
 for “*Quantum theory of polariton weak lasing and polarization bifurcations*”  
 by Huawei Xu, Timothy C. H. Liew, and Yuri G. Rubo

The equation for the density matrix

$$\frac{d\hat{\rho}}{dt} \equiv \mathcal{L}\hat{\rho} = -i[\hat{H}_s, \hat{\rho}] - \frac{W}{2}([\hat{a}, \hat{a}^\dagger \hat{\rho}] + [\hat{b}, \hat{b}^\dagger \hat{\rho}] + \text{h.c.}) - \frac{(\Gamma + \gamma)}{2}([\hat{a}^\dagger, \hat{a} \hat{\rho}] + \text{h.c.}) - \frac{(\Gamma - \gamma)}{2}([\hat{b}^\dagger, \hat{b} \hat{\rho}] + \text{h.c.}), \quad (9)$$

can be used to obtain the equations for the dynamics of the averages of spin operators

$$\hat{s}_0 = \frac{1}{2}(\hat{a}^\dagger \hat{a} + \hat{b}^\dagger \hat{b}), \quad \hat{s}_1 = \frac{1}{2}(\hat{a}^\dagger \hat{a} - \hat{b}^\dagger \hat{b}), \quad \hat{s}_2 = \frac{i}{2}(\hat{a}^\dagger \hat{b} - \hat{b}^\dagger \hat{a}), \quad \hat{s}_3 = \frac{1}{2}(\hat{a}^\dagger \hat{b} + \hat{b}^\dagger \hat{a}). \quad (10)$$

In particular, for the Hamiltonian  $\hat{H}_s = -\varepsilon \hat{s}_1 + (\alpha/2) \hat{s}_3^2$  the averages  $S_\mu = \langle \hat{s}_\mu \rangle \equiv \text{Tr } \hat{\rho} \hat{s}_\mu$  with  $\mu = 0, 1, 2, 3$  define the Stokes vector components and they satisfy the equations

$$\dot{S}_0 = -(\Gamma - W)S_0 - \gamma S_1 + W, \quad (11a)$$

$$\dot{S}_1 = -(\Gamma - W)S_1 - \gamma S_0 - \alpha S_{23}, \quad (11b)$$

$$\dot{S}_2 = -(\Gamma - W)S_2 + \varepsilon S_3 + \alpha S_{13}, \quad (11c)$$

$$\dot{S}_3 = -(\Gamma - W)S_3 - \varepsilon S_2, \quad (11d)$$

where we defined the averages of normal ordered products  $S_{\mu\nu} = \langle : \hat{s}_\mu \hat{s}_\nu : \rangle$ . The dynamics of the tensor  $S_{\mu\nu}$  involves in turn the averages  $S_{\mu\nu\lambda} = \langle : \hat{s}_\mu \hat{s}_\nu \hat{s}_\lambda : \rangle$ , and so on. The simplest way to break this chain of equations is by replacing  $S_{13} \rightarrow S_1 S_3$  and  $S_{23} \rightarrow S_2 S_3$  in Eqs. (11b,c), which explicitly assumes the second-order coherence to be equal to 1. Below we present the results of this mean-field approximation by analyzing the bifurcations of the fixed points of Eqs. (11) under these substitutions in the region of pumping rates  $0 < W < \Gamma$ , assuming also  $0 < \gamma < \Gamma$  and  $\varepsilon > 0$ .

For small  $W$  there is only one static solution, which corresponds to formation of the condensate in the Y linearly-polarized state, defined by the  $b$  annihilation operator. The values of the spin components are

$$S_0 = \frac{W}{2} \left( \frac{1}{\Gamma + \gamma - W} + \frac{1}{\Gamma - \gamma - W} \right), \quad (12a)$$

$$S_1 = \frac{W}{2} \left( \frac{1}{\Gamma + \gamma - W} - \frac{1}{\Gamma - \gamma - W} \right) < 0, \quad S_2 = S_3 = 0. \quad (12b)$$

It can be shown by making small perturbation of equations around this fixed point and performing linear stability analysis that this condensate is unstable for  $W > W_c$ , where critical pumping value  $W_c$  corresponds to  $\alpha\varepsilon|S_1| = (\Gamma - W)^2 + \varepsilon^2$  and can be found as the root of equation

$$[(\Gamma - W_c)^2 - \gamma^2][(\Gamma - W_c)^2 + \varepsilon^2] = \alpha\gamma\varepsilon W_c. \quad (13)$$

There is a pitchfork bifurcation at  $W = W_c$ , which results in appearance of two stable symmetry breaking fixed points for  $W > W_c$ , describing the possibility of formation of two elliptically polarized condensates with positive ( $S_3 > 0$ ) and negative ( $S_3 < 0$ ) handedness. The components of the Stokes vector in this case are

$$S_1 = -\frac{(\Gamma - W)^2 + \varepsilon^2}{\alpha\varepsilon}, \quad (14a)$$

$$S_2 = -\frac{(\Gamma - W)}{\varepsilon} S_3, \quad (14b)$$

$$S_3 = \pm \frac{\gamma}{(\Gamma - W)} \left[ W - \frac{[(\Gamma - W)^2 - \gamma^2][(\Gamma - W)^2 + \varepsilon^2]}{\alpha\gamma\varepsilon} \right]^{1/2}, \quad (14c)$$

$$S_0 = \frac{1}{(\Gamma - W)} \left[ W + \frac{\gamma[(\Gamma - W)^2 + \varepsilon^2]}{\alpha\varepsilon} \right]. \quad (14d)$$

The Stokes components as functions of  $W$  are shown in Fig. 5, taking the positive value of  $S_3$  in Eq. (14c).

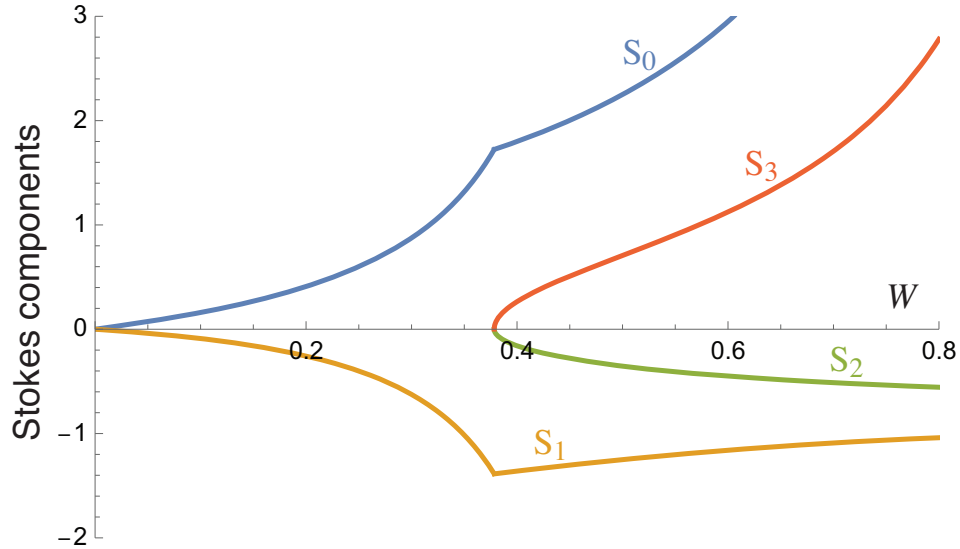


FIG. 5. Showing the dependences of the spin components on the pumping  $W$ . The parameters are  $\Gamma = 1$ ,  $\gamma = 0.5$ ,  $\varepsilon = 1$ , and  $\alpha = 1$ , and they correspond to the bifurcation value  $W_c = 0.378$ .